Lineshapes in magnetic resonance spectra

2000 J. Phys.: Condens. Matter 12 9347

(http://iopscience.iop.org/0953-8984/12/44/315)

J. Phys.: Condens. Matter **12** (2000) 9347–9360. Printed in the UK PII: S0953-8984(00)15595-X

Lineshapes in magnetic resonance spectra

René Berger, Jean-Claude Bissey and Janis Kliava†

Centre de Physique Moléculaire Optique et Hertzienne, UMR Université Bordeaux I–CNRS 5798, Université Bordeaux I, 351 cours de la Libération, 33405 Talence Cédex, France

E-mail: jkliava@frbdx11.cribx1.u-bordeaux.fr

Received 18 July 2000, in final form 20 September 2000

Abstract. In magnetic resonance, and in particular, in superparamagnetic resonance studies at variable temperatures, a correlation between the apparent resonance magnetic field and the apparent linewidth is often observed. In order to account for this correlation, we consider the resonance lineshapes resulting from different phenomenological equations of damped motion of the magnetic moments in the cases of a linear paramagnet and of a perfect soft ferromagnet. The Bloch–Bloembergen, modified Bloch, Gilbert, Landau–Lifshitz and Callen equations are analysed. In most cases we obtain analytical expressions for the apparent resonance-field shift. Finally, we report an experimental variable-temperature study of the superparamagnetic resonance of ultrafine Fe_2O_3 particles in sol–gel glass. Computer simulations using the Landau–Lifshitz lineshape provide good fits of the resonance spectra at different temperatures for the same magnetic and morphological parameters of the particles.

1. Introduction

In theoretical modelling, and in particular in numerically computer fitting magnetic resonance spectra, the notion of *resonance line broadening* should be treated separately from that of the *distribution of resonance magnetic fields*. Such an approach is particularly useful in the case of systems with static disorder. One may first define a weighted distribution of the resonance magnetic fields $\mathcal{P}(B_{\rm res}, \Theta, \Phi, \Psi)$ with the set of Euler angles $(\Theta \quad \Phi \quad \Psi)$ describing the orientation of the *macroscopic* axes of the sample, e.g., the crystallographic axes, with respect to the static and microwave magnetic field, as follows:

$$\mathcal{P}(B_{\rm res,}\Theta, \Phi, \Psi) = \sum_{i,j} \int P(\boldsymbol{H}, \boldsymbol{\Omega}) W_{ij}(\boldsymbol{H}, \boldsymbol{\Omega}) \delta [B_{\rm res} - B_{\rm res}(\boldsymbol{H}, \boldsymbol{\Omega})] \, {\rm d}V(\boldsymbol{H}, \boldsymbol{\Omega}). \tag{1}$$

In equation (1) the random vector $\boldsymbol{H}$ summarizes the ensemble of magnetic (spin-Hamiltonian) parameters (in the case of electron paramagnetic resonance (EPR) of individual paramagnetic centres) and morphological (size and shape) characteristics of magnetic particles (in the case of ferromagnetic resonance (FMR) or superparamagnetic resonance (SPR) in an assembly of magnetically ordered fine particles). The second set of Euler angles $\boldsymbol{\Omega} = (\vartheta \quad \varphi \quad \psi)$ describes the orientation of the *local* magnetic axes with respect to the macroscopic ones. $P(\boldsymbol{H}, \boldsymbol{\Omega})$ is the corresponding joint distribution density and $W_{ij}(\boldsymbol{H}, \boldsymbol{\Omega})$ is the intensity of a particular transition. The integration is performed over distributions of the two random vectors $\boldsymbol{H}$ and $\boldsymbol{\Omega}$. Thus, equation (1) describes the absorption spectrum for infinitely small *intrinsic* linewidth (the Dirac δ-function).

† Author to whom any correspondence should be addressed. Telephone: +33 056 84 61 72; fax: +33 056 84 69 70.

0953-8984/00/449347+14$30.00

At the second stage, $\mathcal{P}(B_{\rm res}, \Theta, \Phi, \Psi)$ is convoluted with a lineshape $F[B - B_{\rm res}, \Delta_B(B_{\rm res}, \Theta, \Phi, \Psi)]$ describing various broadening mechanisms not explicitly taken into account in $P(\boldsymbol{H}, \boldsymbol{\Omega})$. This results in the following absorption intensity:

$$\mathcal{S}(B, \Theta, \Phi, \Psi) = \int_{-\infty}^{\infty} \mathcal{P}(B_{\rm res}, \Theta, \Phi, \Psi) F[B - B_{\rm res}, \Delta_B(B_{\rm res}, \Theta, \Phi, \Psi)]\, {\rm d}V(B_{\rm res}, \boldsymbol{\Omega}). \quad (2)$$

$\Delta_B(B_{\rm res}, \Theta, \Phi, \Psi)$ is the individual linewidth for a paramagnetic centre or particle.

In experimental magnetic resonance studies at variable temperatures, a correlation between the *apparent* resonance magnetic field and the *apparent* (peak-to-peak) linewidth is often observed. In particular, in the case of SPR at low temperatures, resonance spectra broaden in a very spectacular way and shift to lower magnetic fields. Such a behaviour was reported in the SPR of silica-supported nickel particles [1], dispersed ultrafine Mn–Zn ferrite particles [2], nanoscale FeOOH particles [3], nanoparticles of Co stabilized in a polymer [4] and maghemite (γ-Fe_2O_3) nanoparticles in ferrofluids [5]. We have observed a similar tendency for crystallized nanoparticles of Fe_2O_3 in a sol–gel glass system, as reported in section 3.

The superparamagnetism is observed in systems of magnetically ordered fine particles (nanoparticles) dispersed in a diamagnetic matrix. The general approach to the analysis of SPR spectra has been outlined in a recent series of papers [6–9]. The resonance magnetic field of a given particle includes anisotropic contributions, such as those of a magnetocrystalline anisotropy field and a demagnetizing field. Also, at low temperatures the resonance of individual magnetic particles occurs with a considerable linewidth. As a result, the magnetic resonance spectra of an assembly of randomly oriented particles are broadly distributed. At elevated temperatures, thermal fluctuations of magnetic moments severely reduce both the angular anisotropy of resonance magnetic fields and the individual linewidths, so for nanoparticles, superparamagnetic spectral narrowing is observed. However, at lower temperatures these fluctuations are frozen out (the blocking phenomenon) and the resonance spectra at low temperatures become very broad (with a linewidth comparable to the resonance field). This means that the usual assumption of narrow resonance lines (leading to Lorentzian-type individual lineshapes) fails and one must consider in more detail the actual lineshapes resulting from the equation of motion of the magnetic moments.

Unfortunately, in spite of a considerable number of works concerned with magnetic resonance lineshapes, most authors limit themselves to the narrow-linewidth case. Moreover, the few broad-lineshape expressions quoted in the literature seem to be erroneous, *vide ultra*. Thus, the main object of this publication is to remedy the lack of a detailed and systematic analysis of broad resonance lineshapes engendered by different phenomenological equations of motion. We believe that this analysis may be of a general interest to people concerned with magnetic resonance spectroscopy.

The structure of the present paper is as follows. Section 2 provides a survey of different phenomenological equations describing the damping of magnetic moments. We obtain and analyse the corresponding lineshapes and shifts between the 'true' and apparent resonance fields. Section 3 is concerned with our experimental variable-temperature study of superparamagnetic resonance spectra of ultrafine nanoparticles in sol–gel glass and illustrates the pertinence of the above analysis.

2. Phenomenological equations for the relaxation process and lineshapes

If one neglects damping, the motion of the magnetization vector $\boldsymbol{M}$ is described by the magnetic torque equation

$$\dot{\boldsymbol{M}} = \gamma \boldsymbol{M} \wedge \boldsymbol{B}_{\rm eff} \quad (3)$$

where $\boldsymbol{B}_{\text{eff}}$ is the effective magnetic field and γ is the gyromagnetic ratio. In the general case, $\boldsymbol{B}_{\text{eff}}$ includes the applied *static* and *microwave* magnetic fields as well as internal fields, namely the demagnetizing field and the magnetocrystalline anisotropy field. We choose a coordinate system where the static component of $\boldsymbol{B}_{\text{eff}}$, henceforth for simplicity denoted as $\boldsymbol{B}$, and the corresponding magnetization $\boldsymbol{M}_0$ are along the z-axis; the microwave magnetic field lies in the perpendicular plane, $\boldsymbol{b} = (\, b_x \quad b_y \,)$.

In order to account for the relaxation of magnetic moments, a damping term must be added to the right-hand side of equation (3). This term characterizes the torque that tends to align the magnetization with its equilibrium orientation. The physical mechanisms of the relaxation are quite complicated [10], so some phenomenological form of this term is used. Below, we consider successively the cases of Bloch–Bloembergen [11, 12], modified Bloch [13, 14], Gilbert [15], Landau–Lifshitz [16] and Callen [17] equations.

The phenomenological equations have been resolved using the Polder tensor method (p 586 of [10]). The magnetization response to $\boldsymbol{b}$, $\boldsymbol{m} = (\, m_x \quad m_y \,)$, is expressed as

$$\boldsymbol{m} = \begin{pmatrix} \chi & -\mathrm{i}\kappa \\ \mathrm{i}\kappa & \chi \end{pmatrix} \boldsymbol{b} \tag{4}$$

where χ and κ describe, respectively, the response to the x- and y-components of b.

In the case of a circularly polarized microwave field $\boldsymbol{b}^{\pm} = \boldsymbol{b}_0 \mathrm{e}^{\pm \mathrm{i}\omega t}$ (the $\pm$ signs stand for the two polarization directions), the dynamic susceptibility is given by

$$\chi_{\pm} = \chi \mp \kappa = \chi'_{\pm} - \mathrm{i}\chi''_{\pm}.$$

The two polarization directions are usually referred to as 'resonant', or 'Larmor', and 'non-resonant', or 'anti-Larmor', polarizations. For a linearly polarized microwave field $\boldsymbol{b} = \boldsymbol{b}_0 \cos \omega t$ applied along the x-axis, the complex susceptibility is

$$\chi = \chi' - \mathrm{i}\chi'' = \tfrac{1}{2}(\chi_+ + \chi_-) = \tfrac{1}{2}[\chi'_+ + \chi'_- - \mathrm{i}(\chi''_+ + \chi''_-)].$$

The magnetic resonance *absorption* signal is proportional to the imaginary part of the dynamic susceptibility. We obtained analytical forms of the resonance lineshape for the linear polarization and both circular polarization directions of the microwave radiation. One can easily check that in all above-quoted cases, $\chi''(B) = \frac{1}{2}\left[\chi''_+(B) + \chi''_-(B)\right]$. Whenever possible, $\chi''(B)$ has been normalized to unity [18]:

$$\int_{-\infty}^{\infty} \chi''(B)\, \mathrm{d}B = 1. \tag{5}$$

Two different cases of magnetic behaviour of the system have been considered:

(i) that of a linear paramagnet characterized by static magnetization directly proportional to the static magnetic field, $M_0 = \chi_0 B$;
(ii) that of a perfect soft ferromagnet characterized by a stepwise dependence $M_0(B) = M_0 \operatorname{sgn}(B)$ with $M_0 =$ constant.

The expressions given above are concerned with a magnetic field sweep experiment. The resonance magnetic field is defined as $B_0 = -\omega/\gamma$. The static magnetic field is supposed to be much stronger than the microwave magnetic field, so strictly speaking these expressions fail in the immediate vicinity of $B = 0$. The linewidth parameter Δ_B is defined as the half-width at half-height in the narrow-line limit, $\Delta_B \ll B_0$.

The different absorption lineshapes are displayed in figure 1 for the linear polarization and 'resonant' circular polarization. The corresponding derivative-of-absorption lineshapes in the linear polarization case (the most current experimental situation) are shown in figure 2.

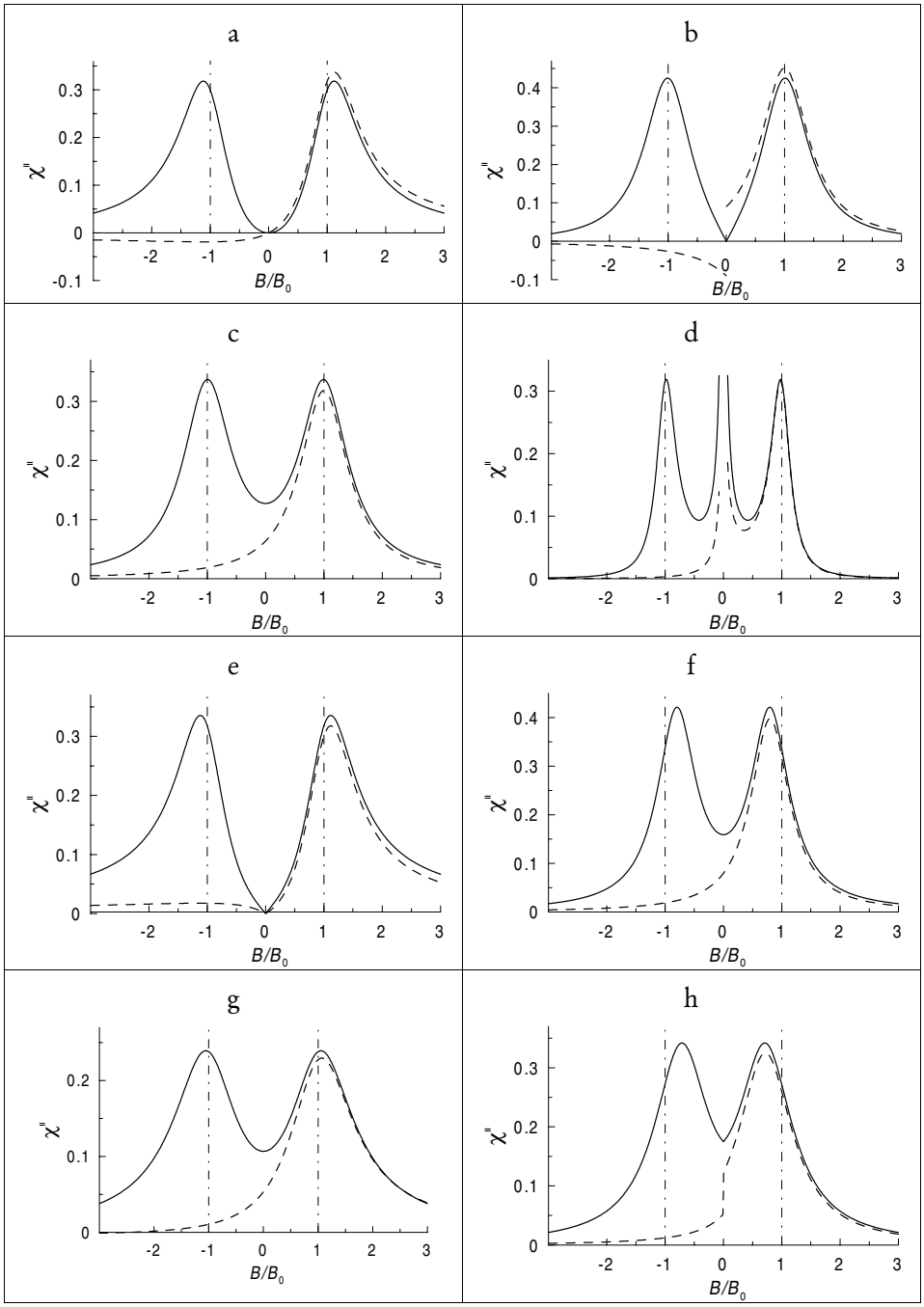

Figure 1. Magnetic resonance absorption lineshapes obtained with different equations of motion: (a) Bloch–Bloembergen, case (i), equation (7); (b) Bloch–Bloembergen, case (ii), equation (10); (c) modified Bloch, case (i), Gilbert, case (ii), Landau–Lifshitz, case (i), equation (14); (d) modified Bloch, case (ii), equation (18); (e) Gilbert, case (i), equation (22); (f) Landau–Lifshitz, case (ii), equation (26); (g) Callen, case (i), equation (30); (h) Callen, case (ii), equation (33). The linewidth ratio is $\varepsilon = \Delta_B/B_0 = \frac{1}{2}$ in all cases and $\eta = \delta_B/B_0 = \frac{1}{5}$ for the Callen lineshape. Full line: linear polarization; dashed line: right circular polarization.

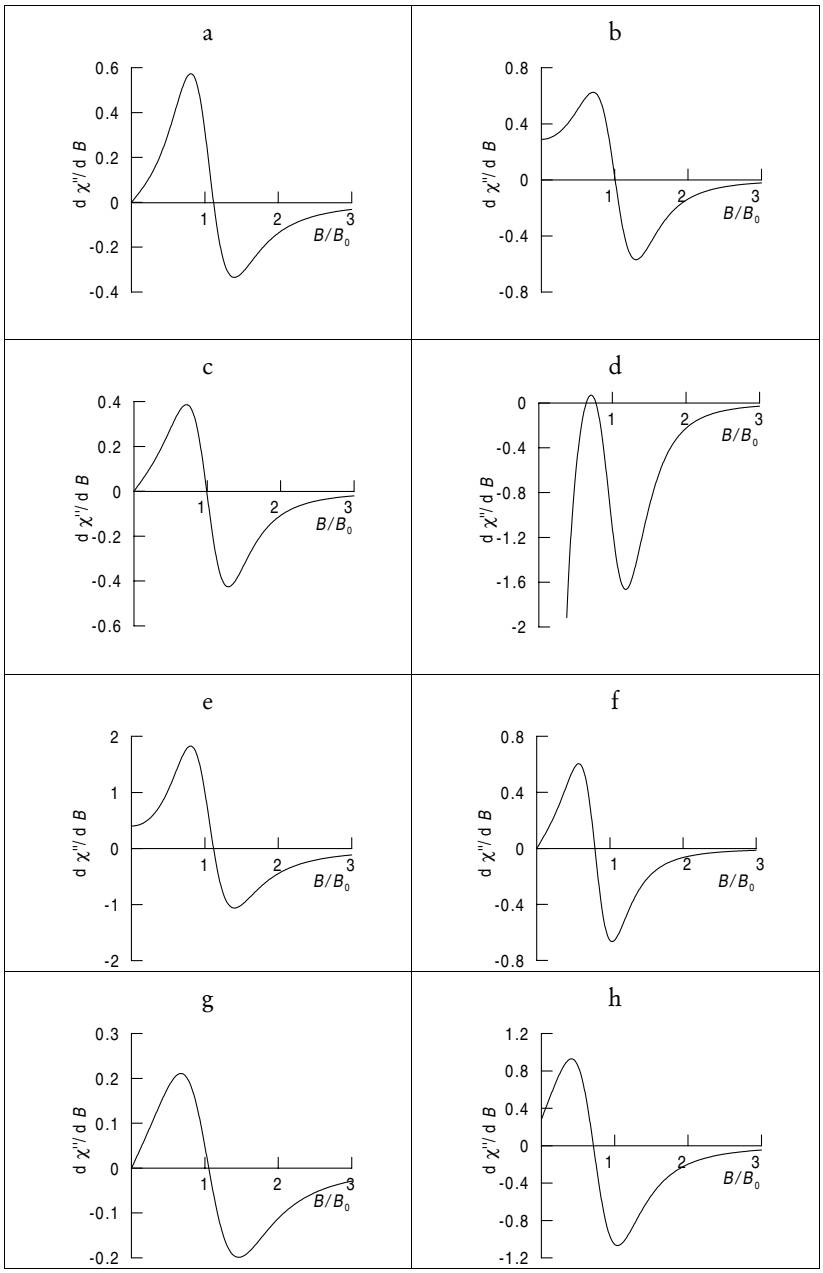

Figure 2. Magnetic resonance derivative-of-absorption lineshapes obtained with different equations of motion (linear polarization): (a) Bloch–Bloembergen, case (i); (b) Bloch–Bloembergen, case (ii); (c) modified Bloch, case (i), Gilbert, case (ii), Landau–Lifshitz, case (i); (d) modified Bloch, case (ii); (e) Gilbert, case (i); (f) Landau–Lifshitz, case (ii); (g) Callen, case (i); (h) Callen, case (ii). The linewidth ratio is $\varepsilon = \Delta_B/B_0 = \frac{1}{2}$ in all cases and $\eta = \delta_B/B_0 = \frac{1}{5}$ for the Callen lineshape.

2.1. The Bloch–Bloembergen equation

Bloembergen adapted Bloch's NMR equation [12] to FMR, as follows:

$$\dot{\boldsymbol{M}} = \gamma \boldsymbol{M} \wedge \boldsymbol{B}_{\text{eff}} - \frac{\boldsymbol{M} - \boldsymbol{\delta}_{iz} M_0}{\boldsymbol{T}} \tag{6}$$

with $\boldsymbol{T} = (\,T_2 \quad T_2 \quad T_1\,)$ and $\boldsymbol{\delta}_{iz} = (\,0 \quad 0 \quad 1\,)$; T_1 and T_2 are referred to, respectively, as the spin–lattice and spin–spin relaxation times.

We define the linewidth as $\Delta_B = 1/|\gamma| T_2$.

In case (i) the following lineshapes are obtained (see figures 1, 2(a)):

$$\chi''(B) = \frac{2}{\pi} \frac{\Delta_B B^2}{\left[(B - B_0)^2 + \Delta_B^2\right]\left[(B + B_0)^2 + \Delta_B^2\right]} \tag{7}$$

$$\chi''_+(B) = \frac{1}{\pi} \frac{\Delta_B B}{B_0\left[(B - B_0)^2 + \Delta_B^2\right]} \tag{8}$$

$$\chi''_-(B) = -\frac{1}{\pi} \frac{\Delta_B B}{B_0\left[(B + B_0)^2 + \Delta_B^2\right]}. \tag{9}$$

The $\chi''(B)$ form of equation (7) is normalized to unity, while those of equations (8) and (9) are divergent.

In case (ii) the normalized lineshapes are (see figures 1, 2(b))

$$\chi''(B) = \frac{B_0 \Delta_B |B|}{\arctan(B_0/\Delta_B)\left[(B - B_0)^2 + \Delta_B^2\right]\left[(B + B_0)^2 + \Delta_B^2\right]} \tag{10}$$

$$\chi''_+(B) = \frac{1}{2} \frac{\Delta_B \operatorname{sgn} B}{\arctan(B_0/\Delta_B)\left[(B - B_0)^2 + \Delta_B^2\right]} \tag{11}$$

$$\chi''_-(B) = -\frac{1}{2} \frac{\Delta_B \operatorname{sgn} B}{\arctan(B_0/\Delta_B)\left[(B + B_0)^2 + \Delta_B^2\right]}. \tag{12}$$

2.2. The modified Bloch equation

The Bloch–Bloembergen equation in the preceding form is unsatisfactory in, at least, two aspects. First, it predicts that no absorption occurs in the absence of the magnetizing field, while such zero-field absorption can be observed experimentally. Second, it leads to the absurd conclusion that far from resonance, *negative* absorption of circularly polarized microwaves should be observed (p 58 of [8], p 152 of [19]), as illustrated in figures 1(a) and 1(b).

In order to avoid these inconsistencies, the Bloch–Bloembergen equation is sometimes modified in such a way that longitudinal relaxation takes place along the direction of the effective magnetic field and lateral relaxation occurs at right angles to it [14]:

$$\dot{\boldsymbol{M}} = \gamma \boldsymbol{M} \wedge \boldsymbol{B}_{\text{eff}} - \frac{\boldsymbol{M} - M_0 \boldsymbol{B}_{\text{eff}}/B}{\boldsymbol{T}}. \tag{13}$$

In case (i) the following normalized lineshapes are obtained (see figures 1, 2(c)):

$$\chi''(B) = \frac{1}{\pi} \frac{\Delta_B (B^2 + B_0^2 + \Delta_B^2)}{\left[(B - B_0)^2 + \Delta_B^2\right]\left[(B + B_0)^2 + \Delta_B^2\right]} \tag{14}$$

$$\chi''_+(B) = \frac{1}{\pi} \frac{\Delta_B}{(B - B_0)^2 + \Delta_B^2} \tag{15}$$

$$\chi''_-(B) = \frac{1}{\pi} \frac{\Delta_B}{(B + B_0)^2 + \Delta_B^2}. \tag{16}$$

Note that for $B = 0$ in the case of linearly polarized radiation one gets

$$\chi''(0) = \frac{1}{\pi}\frac{\Delta_B}{(B_0^2 + \Delta_B^2)} = \frac{1}{\pi}\frac{|\gamma|T_2}{1 + \omega^2 T_2^2} \tag{17}$$

in accordance with the Debye formula for zero-field absorption [14, 20].

In case (ii) the resonance signal shapes are as follows (they are divergent at $B = 0$; see figures 1, 2(d)):

$$\chi''(B) \propto \frac{M_0 B_0 \Delta_B (B^2 + B_0^2 + \Delta_B^2)}{|B|\left[(B - B_0)^2 + \Delta_B^2\right]\left[(B + B_0)^2 + \Delta_B^2\right]} \tag{18}$$

$$\chi''_+(B) \propto \frac{M_0 B_0 \Delta_B}{|B|\left[(B - B_0)^2 + \Delta_B^2\right]} \tag{19}$$

$$\chi''_-(B) \propto \frac{M_0 B_0 \Delta_B}{|B|\left[(B + B_0)^2 + \Delta_B^2\right]}. \tag{20}$$

2.3. The Gilbert equation

Gilbert [15] suggested an equation of motion with a relaxation rate proportional to the total $\dot{\boldsymbol{M}}$:

$$\dot{\boldsymbol{M}} = \gamma \boldsymbol{M} \wedge \boldsymbol{B}_{\text{eff}} + \frac{G}{|\boldsymbol{M}|}\boldsymbol{M} \wedge \dot{\boldsymbol{M}} \tag{21}$$

with $G > 0$. We define the linewidth parameter as $\Delta_B = G B_0$.

In case (i) one gets (see figures 1, 2(e); these lineshapes are not normalized since the corresponding integrals are divergent):

$$\chi''(B) \propto \frac{\chi_0 \Delta_B (B^2 + B_0^2 + \Delta_B^2)\,|B|}{\left[(B - B_0)^2 + \Delta_B^2\right]\left[(B + B_0)^2 + \Delta_B^2\right]} \tag{22}$$

$$\chi''_+(B) \propto \frac{\chi_0 \Delta_B |B|}{(B - B_0)^2 + \Delta_B^2} \tag{23}$$

$$\chi''_-(B) \propto \frac{\chi_0 \Delta_B |B|}{(B + B_0)^2 + \Delta_B^2}. \tag{24}$$

In case (ii) the normalized lineshapes are exactly the same as those obtained with the modified Bloch equation in case (i); see equations (14), (15), (16) and figures 1, 2(c).

2.4. The Landau–Lifshitz equation

Landau and Lifshitz [16] suggested a damping term with the relaxation rate proportional to the precessional component of $\dot{\boldsymbol{M}}$:

$$\dot{\boldsymbol{M}} = \gamma \boldsymbol{M} \wedge \boldsymbol{B}_{\text{eff}} - \frac{\lambda}{|\boldsymbol{M}|^2}\boldsymbol{M} \wedge (\boldsymbol{M} \wedge \boldsymbol{B}_{\text{eff}}) \tag{25}$$

where $\lambda > 0$. It can be shown (see p 153 of [19], p 57 of [21], [22]) that the equations (25) and (21) are equivalent from the mathematical viewpoint if one renormalizes the gyromagnetic ratio in equation (21) as follows: $\gamma' = \gamma(1 + G^2)$. If the damping is small, the Gilbert and Landau–Lifshitz approaches become equivalent from the physical viewpoint, as well.

In case (i), with the linewidth parameter defined as $\Delta_B = \lambda/(|\gamma|\chi_0)$, we obtain exactly the same normalized lineshape expressions as with the Gilbert equation case (ii) and with the modified Bloch equation case (i); see equations (14), (15), (16) and figures 1, 2(c).

In case (ii), noting that $\Delta_B = \lambda B_0/|\gamma||M_0|$, the following normalized lineshapes are obtained (see figures 1, 2(f)):

$$\chi''(B) = \frac{1}{\pi}\frac{B_0^2\Delta_B\left[(B_0^2+\Delta_B^2)B^2+B_0^4\right]}{\left[(B-B_0)^2B_0^2+\Delta_B^2B^2\right]\left[(B+B_0)^2B_0^2+\Delta_B^2B^2\right]} \tag{26}$$

$$\chi_+''(B) = \frac{1}{\pi}\frac{B_0^2\Delta_B}{(B-B_0)^2B_0^2+\Delta_B^2B^2} \tag{27}$$

$$\chi_-''(B) = \frac{1}{\pi}\frac{B_0^2\Delta_B}{(B+B_0)^2B_0^2+\Delta_B^2B^2}. \tag{28}$$

2.5. The Callen equation

The Callen [17] dynamical equation with damping has been obtained using a quantum mechanical approach by quantizing the spin waves into magnons:

$$\dot{\boldsymbol{M}} = \gamma\boldsymbol{M}\wedge\boldsymbol{B}_{\text{eff}} - \frac{\lambda}{|\boldsymbol{M}|^2}\boldsymbol{M}\wedge(\boldsymbol{M}\wedge\boldsymbol{B}_{\text{eff}}) - \alpha\boldsymbol{M}. \tag{29}$$

Note that the first damping term in this equation coincides with the Landau–Lifshitz one, equation (25), while the second one has the same form as the Bloch–Bloembergen one, equation (6), in the case of the lateral relaxation, if one puts $\alpha = 1/T_2$.

In case (i), noting that $\Delta_B = \lambda/|\gamma|\chi_0$ and $\delta_B = \alpha/|\gamma|$, we obtain the following normalized lineshapes (see figures 1, 2(g)):

$$\chi''(B) = \frac{1}{\pi}\frac{(\Delta_B+2\delta_B)B^2+\Delta_B\left[B_0^2+(\Delta_B+\delta_B)^2\right]}{\left[(B-B_0)^2+(\Delta_B+\delta_B)^2\right]\left[(B+B_0)^2+(\Delta_B+\delta_B)^2\right]} \tag{30}$$

$$\chi_+''(B) = \frac{1}{\pi}\frac{\Delta_BB_0+\delta_BB}{B_0\left[(B-B_0)^2+(\Delta_B+\delta_B)^2\right]} \tag{31}$$

$$\chi_-''(B) = \frac{1}{\pi}\frac{\Delta_BB_0-\delta_BB}{B_0\left[(B+B_0)^2+(\Delta_B+\delta_B)^2\right]}. \tag{32}$$

In case (ii), with $\Delta_B = \lambda B_0/|\gamma|M_0$ and $\delta_B = \alpha/|\gamma|$, the lineshapes are (see figures 1, 2(h)):

$$\chi''(B) = \frac{1}{N}\frac{B_0^2\left[(B_0^2+\Delta_B^2)(\Delta_BB^2+2B_0\delta_B|B|)+(B_0^2+\delta_B^2)B_0^2\Delta_B\right]}{\left[(B-B_0)^2B_0^2+(\Delta_B|B|+\delta_BB_0)^2\right]\left[(B+B_0)^2B_0^2+(\Delta_B|B|+\delta_BB_0)^2\right]} \tag{33}$$

$$\chi_+''(B) = \frac{1}{N}\frac{B_0^2(\Delta_B+\delta_B\,\text{sgn}\,B)}{(B-B_0)^2B_0^2+(\Delta_B|B|+\delta_BB_0)^2} \tag{34}$$

$$\chi_-''(B) = \frac{1}{N}\frac{B_0^2(\Delta_B-\delta_B\,\text{sgn}\,B)}{(B+B_0)^2B_0^2+(\Delta_B|B|+\delta_BB_0)^2} \tag{35}$$

where

$$N = \pi - \arctan\frac{B_0^2+\Delta_B\delta_B}{B_0(\Delta_B-\delta_B)} + \arctan\frac{B_0^2-\Delta_B\delta_B}{B_0(\Delta_B+\delta_B)}. \tag{36}$$

2.6. Discussion of the lineshapes; apparent shift of the resonance field

The same resonance lineshape as that described by equations (14), (15), (16) has been reported by Rojo *et al* (equations (5) and (6) of [23]); however, these authors do not specify the equation of motion used to deduce it.

In a recent paper [24], Flores *et al* give three different expressions allegedly corresponding to the Bloch–Bloembergen, Landau–Lifshitz and Gilbert lineshapes, respectively—their equations (5), (6) and (7). These authors do not specify the relation between the static magnetic field and the corresponding magnetization used by them. Note also that the $\chi''_{\max}$-parameter used by these authors does not correspond to the maximum value of χ'' in the case of equations (6) and (7) of [24].

All three equations describe odd functions of the static magnetic field, denoted as H in [24], so H must be replaced by $|H|$ in order to achieve consistency with elementary physical considerations. Indeed, the absorption of *linearly* polarized microwaves must be an even function of the applied static magnetic field. Thus amended, expression (5) of [24] describes the same lineshape as our equation (10) (the Bloch–Bloembergen lineshape in case (ii), that of a perfect soft ferromagnet). On the other hand, expression (6) of [24], contrary to the assertion of the authors, is a solution not of the Landau–Lifshitz equation but of the Gilbert equation for a linear paramagnet—compare with our equation (22). In contrast, expression (7) of [24] given by Flores *et al* can be derived neither from the Gilbert equation nor from the Landau–Lifshitz equation, though it looks very like a solution of the latter. Indeed, one can readily show that it results from solving the Landau–Lifshitz equation with (erroneous) neglect of the microwave component $\boldsymbol{b}$ of the effective magnetic field $\boldsymbol{B}$ in the damping term.

Most often, simplified expressions of the resonance lineshapes are considered, valid at low damping rate, and hence corresponding to narrow linewidth, $\Delta_B \ll B_0$. In this instance the applied static field B is swept only in the vicinity of B_0, and one gets essentially the same (Lorentzian) lineshape in all cases considered above, namely

$$\chi''(B) = \frac{1}{\pi}\frac{\Delta_B}{(B - B_0)^2 + \Delta_B^2} \tag{37}$$

(in the case of the Callen equation, Δ_B should be replaced by $\Delta_B + \delta_B$). In this approximation the distinction between the responses to the linear and right-polarized microwave radiation disappears.

Here we are interested instead in the case of broad resonance lines, so the difference between various approaches becomes crucial. One can see from figures 1 and 2 that a considerable apparent shift of the resonance position occurs for some lineshapes. In some cases one can obtain analytical expressions for this shift as a function of the linewidth. In the subsequent expressions $B_{\max}$ denotes the maximum of the resonance line (corresponding to the zero level in the experimentally recorded derivative-of-absorption line) and $\varepsilon = \Delta_B/B_0$.

- For the Bloch–Bloembergen lineshape in case (i) (see equation (7)) and for the Gilbert lineshape in case (i) (see equation (22)), one gets

$$\frac{B_{\max}}{B_0} = \sqrt{1 + \varepsilon^2}. \tag{38}$$

- For the Bloch–Bloembergen lineshape in case (ii) (see equation (10)), one gets

$$\frac{B_{\max}}{B_0} = \frac{1}{\sqrt{3}}\sqrt{2\sqrt{1 + \varepsilon^2 + \varepsilon^4} + 1 - \varepsilon^2}. \tag{39}$$

- For the modified Bloch lineshape in case (i), the Gilbert lineshape in case (ii) and the Landau–Lifshitz lineshape in case (i) (see equation (14)), one gets

$$\frac{B_{\max}}{B_0} = \sqrt{2\sqrt{1 + \varepsilon^2} - 1 - \varepsilon^2}. \tag{40}$$

- For the modified Bloch lineshape in case (ii) only relatively narrow linewidth needs to be considered because of the divergence at $B = 0$. So, in the resonance range, the responses to the linear and right-polarized microwave radiation are very close in shape. With the latter response, having much simpler form (cf. equations (18) and (19)), one gets

$$\frac{B_{\max}}{B_0} = \frac{2}{3} + \frac{1}{3}\sqrt{1 - 3\varepsilon^2} \approx 1 - \frac{1}{2}\varepsilon^2 \qquad \varepsilon \leqslant \frac{\sqrt{3}}{3}. \tag{41}$$

- For the Landau–Lifshitz lineshape in case (ii) (see equation (26)), one gets

$$\frac{B_{\max}}{B_0} = \frac{\sqrt{2\sqrt{1+\varepsilon^2} - 1 - \varepsilon^2}}{1+\varepsilon^2}. \tag{42}$$

- For the Callen lineshape in case (i) (see equation (30)), noting additionally that $\eta = \delta_B/B_0$, one gets

$$\left(\frac{B_{\max}}{B_0}\right)^2 = \frac{2(1+\eta/\varepsilon)\sqrt{\left[1+(\varepsilon+\eta)^2\right](1+\eta^2)} - 1 - (\varepsilon+\eta)^2}{1+2\eta/\varepsilon}. \tag{43}$$

Figure 3 shows graphs of $B_{\max}/B_0$ as a function of ε for some lineshapes. One can see in the left-hand part of this figure that as ε increases, the apparent resonance positions of the Bloch–Bloembergen lineshape cases (i), (ii) and Gilbert lineshape case (i) shift towards high fields. In contrast, those of the modified Bloch case (i), Gilbert case (ii) and Landau–Lifshitz lineshape cases (i), (ii) shift downwards, this tendency being particularly pronounced for the latter case. (For the Callen lineshape case (ii), the shift of the resonance is still more striking, as one can see from figures 1, 2.) The latter tendency is most interesting since it corresponds to that observed with the experimental SPR spectra. In the right-hand part of figure 3 we show the apparent shift of the resonance field for the Callen lineshape case (i) for different values of η/ε (the case with $\eta/\varepsilon = 0$ coincides with curve (c) in the left-hand part of this figure).

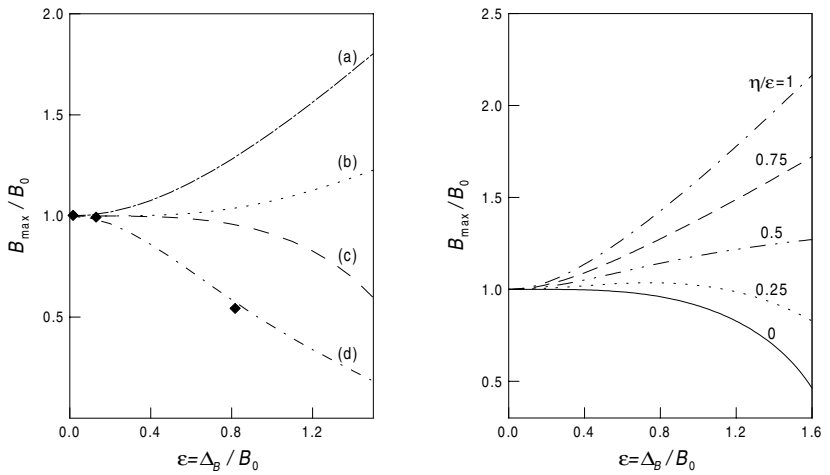

Figure 3. Left: apparent resonance shift B/B_0 versus the linewidth ratio ε for various lineshapes: (a) Bloch–Bloembergen, case (i), Gilbert, case (i), equation (38); (b) Bloch–Bloembergen, case (ii), equation (39); (c) modified Bloch, case (i), Gilbert, case (ii), Landau–Lifshitz, case (i), equation (40); (d) Landau–Lifshitz, case (ii), equation (42). Right: apparent resonance shift B/B_0 versus the linewidth ratio ε calculated for the Callen lineshape case (i), equation (43), and various values of the ratio η/ε. The results of computer simulations of the experimental spectra (see the text) are indicated by the symbols ♦.

3. Experimental procedure, computer simulations and discussion

In this section we analyse the temperature dependence of the X-band SPR spectra of ultrafine nanoparticles in sol–gel glass.

The sol–gel mixture was prepared as described in [25]. Iron was added to the mixture in the form of aqueous nitrate in order to obtain a Fe/Si molar ratio of 1%. The sample was treated in air at 1000 °C for six hours to obtain silica glass with γ-Fe_2O_3 nanoparticles, as confirmed by x-ray diffraction. The spectra were measured between 300 and 15 K using a Bruker EMX spectrometer provided with an ER4112HV variable-temperature unit. The measurement temperature was determined with an uncertainty of ± 0.5 K.

As temperature lowers, one observes a decrease of the resonance-field value and a concomitant increase of the linewidth, as shown in figure 4 for two limiting temperatures. (The data for intermediate temperatures will be considered in detail elsewhere.)

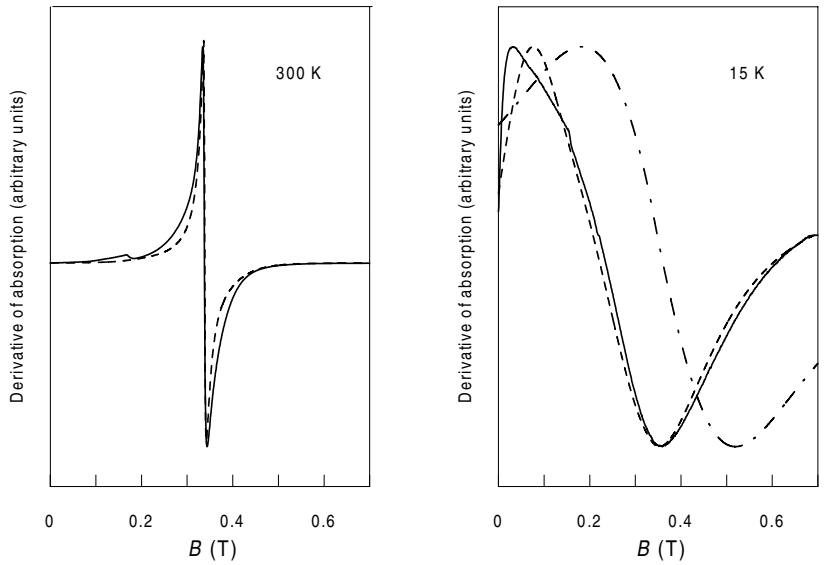

Figure 4. Simulations of the experimental SPR spectra (full lines) at 300 K (left) and 15 K (right). The dashed and dash–dotted lines are the best-fit computer-generated SPR spectra for the Landau–Lifshitz case (ii) and Lorentzian lineshapes, respectively. (At 300 K the two simulated spectra practically coincide.)

In order to extract the characteristics of the individual linewidth, the spectra were computer simulated using the following expression for the SPR spectrum of an assembly of particles with distributed diameters D [6–9]:

$$I(B) = \int_{\varphi}\int_{\vartheta}\int_{D} F\left[B - B_{res}(D, \vartheta, \varphi), \Delta_B\right] f_V(D) \sin\vartheta \, \mathrm{d}D \, \mathrm{d}\vartheta \, \mathrm{d}\varphi \qquad (44)$$

where ϑ and φ are the polar and azimuthal angles of $\boldsymbol{B}$ with respect to the crystallographic axes. $f_V(D)$ is the volume fraction of particles with diameter D and volume V given by $f_V(D) = n(D)V/V_t$ where $n(D)$ is their relative number and V_t the total volume of the particles. The distribution of $n(D)$ is usually assumed to have a log-normal form and it can be shown that in this case $f_V(D)$ is also a log-normal distribution with the same standard

deviation of ln D, σ:

$$f_V(D) = \frac{\exp(-\sigma^2/2)}{\sqrt{2\pi}\sigma D_{V_{\max}}} \exp\left[-\frac{1}{2\sigma^2}\ln^2\frac{D}{D_{V_{\max}}}\right] \tag{45}$$

where $D_{V_{\max}}$ corresponds to the maximum of $f_V(D)$.

In a recent investigation on the SPR of nanoparticles at different temperatures [9], we have shown that the pronounced temperature dependence of the individual linewidth Δ_B can be well fitted by

$$\Delta_B = \Delta_0 L(x) G(y_s). \tag{46}$$

In equation (46) Δ_0 is a saturation linewidth at 0 K, $L(x) = \coth x - 1/x$ is the Langevin function with $x = MVB_{\text{eff}}/kT$, V being the particle volume. $G(y_s)$ is the value of the function

$$G(y) = \frac{P_4(y)}{L(y)} = \left(1 + \frac{35}{y^2}\right)\frac{1}{L(y)} - \frac{10}{y} - \frac{105}{y^3} \tag{47}$$

for $y_s = K_1 V_s/kT$, the ratio of the magnetocrystalline anisotropy energy to the thermal energy for some reference particle of volume V_s, K_1 being the first-order anisotropy constant and $P_4(y)$ the fourth-order Legendre polynomial.

The magnetic parameters of γ-Fe_2O_3 (maghemite) used in computer simulations are: $M_0 = 370$ kA m^{-1} and $K_1 = -4.64$ kJ m^{-3} (cubic symmetry) [26]. The particle shapes were assumed as ellipsoids of revolution characterized by the respective demagnetizing factors $N_\parallel$ and $N_\perp$ in the directions parallel and perpendicular to the major axes. The spectra at different temperatures have been calculated with the following parameters: $\Delta_0 = 0.34$ T, $D_{V_{\max}} = 6.8$ nm, $\sigma = 0.40$, $V_s = 6370$ nm^3, $N_\perp - N_\parallel = 0.33$.

In figure 4 the computer-generated spectra are shown for two different individual lineshapes, the Lorentzian (see equation (37)) and the Landau–Lifshitz case (ii) lineshape (see equation (26)), together with the corresponding experimental spectra. At 300 K the difference between the two lineshapes is not visible (the two computer-generated spectra practically coincide), while at 15 K the spectrum calculated with the Landau–Lifshitz lineshape, in contrast to that calculated with the Lorentzian lineshape, is in good accord with the experimental spectrum.

In figure 3 (left) we have plotted the resonance field versus individual linewidth values extracted from the computer simulations. One can see that the experimental points closely fit the Landau–Lifshitz curve.

With the Lorentzian lineshape, satisfactory fits to the experimental low-temperature spectra can only be attained with additional, rather unphysical, assumptions (e.g., variation with temperature of the form factor $N_\perp - N_\parallel$, etc). On the other hand, as regards the simulation with the Landau–Lifshitz lineshape, the discrepancy from the experimental spectrum in the low-field range can be readily explained by the following facts. First, in the experimental spectra there is a contribution from the EPR signal with the effective g-factor $g_{\text{eff}} \approx 4.3$ arising from isolated Fe^{3+} ions in the glass matrix (this contribution is clearly seen in the 300 K spectrum). Its linewidth being almost temperature-independent, this signal provides a much more important contribution at 15 K, as the main resonance signal is drastically broadened. Second, at low magnetic fields the assumption of field-independent static magnetization is no longer valid. Third, we did not take into account the temperature dependence of the magnetic parameters M_0 and K_1.

In spite of the simplifying assumptions made, the good fit to the experimental low-temperature SPR spectra obtained with the Landau–Lifshitz lineshape seems quite significant.

4. Conclusions

Different phenomenological equations for the damped motion of the magnetic moments, namely, the Bloch–Bloembergen, modified Bloch, Gilbert, Landau–Lifshitz and Callen equations, have been solved for two cases of magnetic behaviour: that of a linear paramagnet and that of a perfect soft ferromagnet. Analytical lineshape expressions have been calculated for both resonant and non-resonant circular polarization as well as for linear polarization of the microwaves. The relations between the magnetic field value at the absorption maximum (the apparent resonance position) and the resonance linewidth are given for different phenomenological equations. The corresponding graphs show that, as the linewidth becomes comparable with the resonance-field value, a conspicuous shift of the apparent resonance position occurs (this shift can be positive or negative depending on the type of the equation of motion).

This analysis has been applied to the case of superparamagnetic nanoparticles of γ-Fe_2O_3 in a sol–gel silica glass. Convincing computer fits of the superparamagnetic resonance spectra at different temperatures have been obtained using the Landau–Lifshitz lineshape (including both resonant and non-resonant contributions). It can be concluded that in this instance the Landau–Lifshitz lineshape provides the most adequate description of the apparent resonance-field shift as a function of the linewidth.

The approach outlined here can be extended to other magnetic systems exhibiting relatively broad resonance lines. That is, the character of the correlation between the apparent resonance fields and the linewidths may guide the choice of an appropriate phenomenological equation and hence of an adequate theoretical lineshape expression.

Acknowledgment

The authors are indebted to C Estournès (IPCMS, Strasbourg) for providing the samples of sol–gel glass used in this work.

References

[1] Sharma V K and Baiker A 1981 *J. Chem. Phys.* **75** 5596
[2] Nagata K and Ishihara A 1992 *J. Magn. Magn. Mater.* **104–107** 1571
[3] Ibrahim M M, Edwards G, Seehra M S, Ganguly B and Huffman G P 1994 *J. Appl. Phys.* **75** 5873
[4] Respaud M 1997 *Thesis* INSA Toulouse
[5] Gazeau F, Bacri J C, Gendron F, Perzynski R, Raikher Yu L, Stepanov V I and Dubois E 1998 *J. Magn. Magn. Mater.* **186** 175
[6] Berger R, Bissey J-C, Kliava J and Soulard B 1997 *J. Magn. Magn. Mater.* **167** 129
[7] Berger R, Kliava J, Bissey J-C and Baïetto V 1998 *J. Phys.: Condens. Matter* **10** 8559
[8] Kliava J and Berger R 1999 *J. Magn. Magn. Mater.* **205** 328
[9] Berger R, Kliava J and Bissey J-C 2000 *J. Appl. Phys.* **87** 7389
[10] Patton C E 1975 *Magnetic Oxides* vol 2, ed D J Craik (New York: Wiley)
[11] Bloch F 1946 *Phys. Rev.* **20** 460
[12] Bloembergen B 1950 *Phys. Rev.* **78** 572
[13] Codrington R S, Olds J D and Torrey H C 1954 *Phys. Rev.* **95** 607
[14] Garstens M A and Kaplan J I 1955 *Phys. Rev.* **99** 459
[15] Gilbert T L 1955 *Phys. Rev.* **100** 1243
[16] Landau L and Lifshitz E 1935 *Phys. Z. Sowjetunion* **8** 153
[17] Callen H B 1958 *J. Phys. Chem. Solids* **4** 256
[18] Poole C P Jr and Farach H A 1971 *Relaxation in Magnetic Resonance* (New York: Academic)
[19] Lax B and Button K J 1962 *Microwave Ferrites and Ferrimagnetics* (New York: McGraw-Hill)
[20] Garstens M A 1954 *Phys. Rev.* **93** 1228

[21] Skrotskii G V and Kurbatov L V 1966 *Ferromagnetic Resonance* ed S V Vonsovskii (Oxford: Pergamon)
[22] Iida S 1963 *J. Phys. Chem. Solids* **4** 625
[23] Rojo M, Margineda J and Muñoz J 1991 *Meas. Sci. Technol.* **2** 141
[24] Flores A G, Torres L, Raposo V, López-Díaz L, Zazo M and Iñiguez J 1999 *Phys. Status Solidi* a **171** 549
[25] Estournès C, Lutz T, Happich J, Quaranta T, Wissler P and Guille J L 1997 *J. Magn. Magn. Mater.* **173** 83
[26] Schmidbauer E and Keller R 1996 *J. Magn. Magn. Mater.* **152** 99